DATA PROCESSING ALGORITHM OF COHERENT WIND MEASUREMENT BASED ON TIME DOMAIN ALIGNMENT

Zhendong WANG[1], Zaihong HOU[2,*], Xu JING[3]

The signal - to - noise ratio (SNR) is a crucial factor influencing the performance of coherent wind lidar. The interference of random noise can be mitigated through the accumulation of multiple pulses. Non - coherent accumulation simply accumulates signals without taking into account their phase relationships. In contrast, a coherent accumulation algorithm, which makes use of the signal's phase information to achieve in - phase superposition of the signal, can more effectively optimize the signal - to - noise ratio. This paper proposes a coherent accumulation algorithm based on time - domain alignment. This algorithm employs correlation coefficients to match and compensate for the modulation of pulse signals, thereby achieving coherence among echoes. Subsequently, accumulation averaging is carried out to obtain an SNR gain. Numerical simulations are performed to evaluate the algorithm's detection ability for echo signals under different amplitude noise interferences. When compared with non - coherent accumulation and direct coherent accumulation algorithms, the proposed algorithm can significantly enhance the signal detection probability. In actual detections, by comparing non - coherent accumulation and direct coherent accumulation algorithms using the radial wind speeds in actual fixed atmospheric regions, the accuracy of real - time signal detection can be optimized. In low - power detections, the algorithm can extract wind speed information with fewer pulse accumulations. Moreover, by combining multiple sets of wind speed data, it can clearly analyze the probability distribution of wind speeds.

The algorithm enables the calculation of simulated wind speeds and the radial wind speeds at fixed atmospheric points and can be effectively applied to the data processing of atmospheric wind fields measured by coherent wind lidar.

Keywords: Wind measurement; Lidar; Coherent detection; Data processing; Signal-to-noise ratio

1. Introduction

The measurement of wind speed in designated areas has important practical significance and application value for laser transmission calculation,

[1] Key Laboratory of Atmospheric Optics, Anhui Institute of Optics and Fine Mechanics, Chinese Academy of Sciences, Hefei 230031; University of Science and Technology of China, Hefei 230026, China

[2] Key Laboratory of Atmospheric Optics, Anhui Institute of Optics and Fine Mechanics, Chinese Academy of Sciences, Hefei 230031; State Key Laboratory of Pulsed Power Laser Technology, Hefei 230031, China, e-mail: zhhou@aiofm.ac.cn

[3] State Key Laboratory of Pulsed Power Laser Technology, Hefei 230031, China

meteorological forecasting research, aircraft takeoff and landing safety warning, and wind power generation site selection [1]. Yu Yongjing and others proposed a set of wind tower layout schemes based on neural network algorithms to increase the development and utilization of wind energy resources [2], which is suitable for representative analysis of wind tower at the wind farm level but will greatly increase costs in other applications. Liu Yang proposed a new type of thermal wind measurement method based on temperature sensor arrays, and designed two types of arrays, namely, cross type and circular type, to achieve fixed point measurement of wind direction and wind speed [3]. It can be applied to extremely harsh environments but cannot effectively achieve real-time measurement of three-dimensional wind fields. Hou Tianhao realized the detection of low altitude wind speed and direction with the help of a multi rotor UAV platform and a wind pressure anemometer [4] but brought about problems such as rotor turbulence correction and flight attitude correction. Zhang Pinghui et al. proposed a non-Doppler lidar wind measurement system based on convolutional neural network technology, which uses a semiconductor coupled device (CCD) to capture the lidar backscatter map of aerosol particles, and achieves quantitative wind speed measurement based on the motion trajectory characteristics of aerosol particles at different wind speeds [5], which can further reduce the initial cost of wind measurement equipment, However, a large amount of data is required to support its training process. Gu Hao has proposed a variety of data processing algorithms based on wind acoustic radars to optimize the measurement of low altitude wind speed [6]. However, considering the characteristics of acoustic waves, wind acoustic radars have a relatively short detection distance and are susceptible to the impact of the atmospheric environment. At night and at high altitudes, the signal to noise ratio is low, requiring a long accumulation time [7].

Laser Coherent Wind Radar detects the backscattered signals of aerosols moving with the wind in the atmosphere to calculate the corresponding Doppler frequency shift information, with strong real-time detection ability and environmental adaptability. The research report on laser coherent wind measurement began in the 1970s with the continuous CO2 lidar system with a wavelength of built by Huffaker et al. and obtained the wind speed of the polluted atmosphere [8]. With the development of laser technology, various types of lasers have emerged [9-11], such as gas lasers, solid state lasers, and fiber lasers. Combining pulse and continuous laser output systems, a series of studies on laser coherent wind lidars have been formed. Data processing is a key part of directly demonstrating system performance. Zhou Yongsheng et al. used the FFT algorithm after zeroing processing to apply to coherent wind lidar frequency estimation. Compared with the commonly used frequency estimation algorithm pulse pair algorithm (PP algorithm) and improved pulse pair algorithm, they verified the obvious advantages of zeroing FFT algorithm in frequency estimation of weak

signals in coherent wind lidar, effectively suppressing the "barrier effect" of traditional FFT algorithm [12], Combining the adjustment of the non coherent cumulative quantity can improve the signal to noise ratio of the echo signal. Li Yunfei used an algorithm of non coherent spectrum accumulation for the corresponding range gate signal, followed by Gaussian fitting, and took the frequency corresponding to the maximum amplitude as the target frequency [13]. Luo Tao adopted a comprehensive algorithm based on Welch power spectrum estimation combined with autocorrelation detection and energy center correction to achieve the estimation of weak low-level atmospheric wind speed signals and obtained experimental results with a wind speed measurement error of 0.27m/s over a distance range of 20m [14]. Yang Wuhao compared various interpolation methods in spectrum correction, optimized spectrum estimation based on the energy center of gravity method and improved the accuracy of algorithm estimation [15]. The maximum likelihood estimation (ML) used by Wang Pingchun estimates wind speed by establishing a logarithmic likelihood function containing system parameters and searching for the frequency parameter corresponding to the maximum value [16]. However, it is necessary to know the correlation function of the logarithmic likelihood function and the specific form of the signal, and the algorithm is relatively complex, resulting in slower real-time processing speed. The Maximum Likelihood Discrete Spectral Peak Estimation (MLDSP) algorithm used by Jin Xiaomei is mainly based on Fast Fourier Transform. It first calculates the power spectrum of the echo signal and then finds the frequency corresponding to the maximum periodogram coefficient to obtain the maximum likelihood solution of the Doppler frequency caused by wind speed [17]. The algorithm has low computational complexity and high time efficiency and is also a commonly used wind speed estimation algorithm for laser coherent wind measurement systems. Liu Feifei inverted the wind speed profile vector measured by laser radar by accumulating the corresponding power spectrum information of each range gate obtained by Fast Fourier Transform (FFT) [18] and then processed to obtain the wind speed information. The above data processing methods are based on the estimation of the frequency domain peak signal after spectrum accumulation to obtain the echo signal. This does not take into account phase information and requires nearly 10000 times of processing to increase the detection probability of the echo signal. Fan Dongqian set up a phase detection system based on orthogonal mixing to eliminate the random initial phase of each pulse cycle to achieve the effect of improving the cumulative signal-to-noise ratio [19], further confirming the effectiveness of the coherent accumulation algorithm in processing weak signals.

In order to better accommodate the characteristics of low - altitude wind fields, which are highly susceptible to external disturbances and exhibit frequent wind speed variations, the echo signals are processed through time - domain alignment. This approach is designed to strengthen the "coherence" among different

pulse periods, thereby achieving a notable improvement in the signal - to - noise ratio. The efficacy of time - domain alignment in the processing of coherent wind measurement data has been further validated. This validation was accomplished by integrating numerical simulations with real - world verification based on the detection of actual atmospheric wind speeds.

2. Structural Design and Analysis of Pulsed Coherent Wind Measurement System

2.1. Overall system framework diagram

The overall optical path of the system is shown in Fig. 1 and mainly consists of four parts: laser generation module, laser transceiver module, signal detection module, and data processing module. In the laser generation module, through polarization maintaining beam splitting, the output signal of the laser is divided into main oscillation light and local oscillation light.

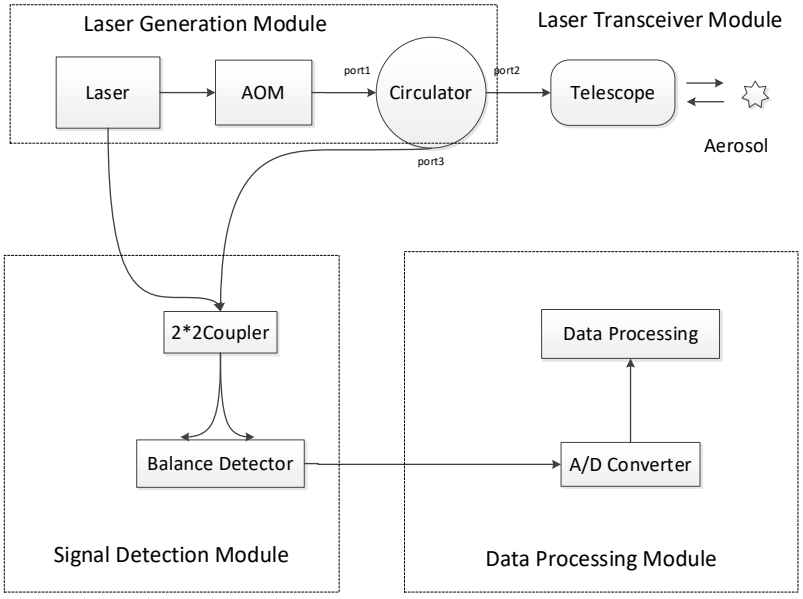

Fig. 1. Principle block diagram of coherent detection system

After frequency shifting and amplification, the main oscillation light enters the port of the circulator and enters the laser transceiver system, while the local oscillation light is directly output to the signal detection module as a single input. The laser transceiver module is mainly a telescope system with an aperture of and a focal length of. On the one hand, it focuses the input main vibration light to detect the target position, on the other hand, it receives the focused laser light and the backscatter signal energy of the aerosol mass moving with the wind in the atmosphere, and outputs the received echo signal to the signal detection module as

another input. The signal detection module is mainly composed of an optical fiber coupler and balanced detector, wherein the input end of the coupler receives the local optical signal and the backscattered signal respectively. The two signals are coupled and enter the balanced detector for frequency mixing. The resulting interference signal is detected and collected before entering the data processing module. After digital to analog conversion, the final frequency shift of the echo signal is analyzed and calculated, thereby corresponding to the radial wind speed.

The system adopts an all-fiber structure design, and the optical fibers and related devices used have polarization maintaining functions, in order to minimize the noise generated by the polarization mismatch between the backscattered signal and the local oscillator signal, thereby improving the signal to noise ratio of the final echo signal. The balance detector used utilizes two detectors with basically identical response parameters. By outputting the difference between the two detectors, the effect of low-frequency relative intensity noise and direct flow on the system's signal-to-noise ratio is eliminated [20].

2.2. Principle Analysis of Coherent Wind Measurement System

Coherent detection is based on the phenomenon that moving objects under the optical Doppler effect produce corresponding frequency changes to the laser signal. Part of the initial laser signal is mixed with the echo signal with Doppler frequency shift, and then relevant data processing is performed to obtain the frequency shift caused by wind speed. Combining the Doppler effect, the corresponding estimation between the frequency shift amount and the motion speed is

$$V = \frac{\Delta f * \lambda}{2 * \cos\theta} \tag{1}$$

In equation (1), Δf is the frequency shift caused by wind speed, and λ is the laser wavelength, θ indicating the angle between the line of sight direction of the laser and the wind direction.

In a coherent wind measurement system, the echo signal is the result of the combined action of aerosol particles moving with the wind. Therefore, during detection, atmospheric turbulence, background noise, and initial acoustooptic frequency shifts can damage the phase of the signal, thereby weakening the "coherence" between the pulse periods. The schematic diagram of a coherent wind measurement system is shown in Fig. 1, and the LO optical signals ultimately participating in the coupling can be represented as:

$$E_L(t) = A_L \sin(2\pi f_L t + \varphi_L) \tag{2}$$

In equation (2), A_L represents the amplitude of the LO optical signal, E_L represents the intensity of the LO optical signal, f_L represents the frequency of the LO optical signal, and φ_L represents the phase of the LO optical signal. The main vibration light emitted by the laser is amplified by frequency shifting and then

collided with an aerosol mass moving with the wind in the air before scattering. The backscattering signal is received by the system to form a backscattering signal participating in the coupling. If the frequency change of the signal is recorded as df , the backscattering signal strength can be shown as:

$$E_S(t) = A_S \sin(2\pi f_S t + \varphi_S) \tag{3}$$

In equation (3), A_S represents the amplitude of the echo signal, E_S represents the strength of the backscattered signal, f_S represents the frequency of the backscattered signal, and φ_S represents the phase of the relatively changed backscattered signal. The signal after mixing the LO signal with the backscattered signal can be expressed as:

$$E(t) = E_S(t) + E_L(t) = A_S \sin(2\pi f_S t + \varphi_S) + A_L \sin(2\pi f_L t + \varphi_L) \tag{4}$$

Thus, the photocurrent of the photodetector

$$\begin{aligned} i(t) \propto \alpha * E^2(t) = \alpha * \{ & \frac{A_S^2}{2} + \frac{A_L^2}{2} + \frac{A_S^2}{2}\cos[2(2\pi f_S t + \varphi_S)] + \\ & \frac{A_L^2}{2}\cos[2(2\pi f_L t + \varphi_L)] + A_S A_L \cos\left[2\pi(f_S + f_L)t + (\varphi_S + \varphi_L)\right] + \\ & A_S A_L \cos\left[2\pi(f_S - f_L)t + (\varphi_S - \varphi_L)\right]\} \end{aligned} \tag{5}$$

In equation (5), α is the photoelectric conversion ratio, which is a constant. The signal that can ultimately be output by the detector without considering the DC component when the detector limits bandwidth.

According to Equation (6), there is a frequency shift caused by wind speed $\Delta f = f_S - f_L - df$, and the corresponding wind speed information can be calculated from the final detected signal through spectrum transformation.

3. Coherent accumulation algorithm based on time domain alignment

3.1. Non coherent accumulation and coherent accumulation

Coherent wind measurement pulse lidar detects signals that emit laser light and are backscattered back through atmospheric aerosols. The echo signal will become weak due to multiple interferences such as energy constraints of emitting a single laser pulse, actual detection distance, round-trip environmental impact, and acquisition equipment noise. In order to effectively extract the frequency information of weak echo signals, multi-pulse accumulation method is commonly used to process the echo signal after spectrum transformation. Multiple accumulation can improve the detection probability of the echo signal. In multi pulse accumulation, non coherent accumulation and coherent accumulation are commonly used processing methods.

Non coherent accumulation is also known as "accumulation after detection", which simply requires aligning and adding the envelope of the pulses. However, due to the lack of use of phase information, the accumulated signal to noise ratio is low, and it is often necessary to rely on nearly 10000 times of accumulation to discover the echo signal. An array of detected signal data with a group of pulses and a data length of each group of pulses is provided, and the non coherent accumulation of the array can be expressed as

$$Y_i = \sqrt{\sum_{j=1}^{N} | X_{ij} |^2} \tag{7}$$

In Equation (7), i is the corresponding pulse sequence number, and X_{ij} is the number of rows and columns in the input array. Coherent accumulation, also known as "pre detection accumulation," preserves phase information in the accumulated data, making it more difficult to achieve than non coherent accumulation. At this point, the coherent accumulation of data arrays can be expressed as

$$Y_i = \sum_{j=1}^{N} X_{ij} \tag{8}$$

The coherent accumulation algorithm is to preserve phase information to superimpose and average the spectral data of multiple sets of pulse corresponding range gate signals. By superposing the spectral data of different pulse signals, phase differences are eliminated, thereby improving the amplitude intensity of the signal accumulation average and optimizing the signal to noise ratio.

3.2. Formation and influence of phase difference between pulses

The main oscillator signal of a coherent laser wind radar will bring a random initial phase to each waveform during the acousto-optic frequency shift and transmission round-trip process. Incomplete coherence will result in errors in the coherent accumulation of the echo signal [17]. In combination with the description in Section 2.2, set $\varphi_0(n)$ as the initial phase of the first pulse signal, and the phase change amount when the pulse signal is received in the test is. Therefore, the phase of the LO optical signal can be expressed as $\Delta\varphi(n)$.

$$\varphi_L(n) = \varphi_0(n) \tag{9}$$

The phase of the backscattered signal participating in the coupling can be expressed as

$$\varphi_S(n) = \varphi_0(n) + \Delta\varphi(n) \tag{10}$$

Here,

$$\varphi_i(n) = \varphi_S(n) - \varphi_L(n) = \Delta\varphi(n) \tag{11}$$

Set noiseless pulse signals $y(n,t) = \sin(2\pi ft + b(n))$, where n is pulse ordinal numbers, taken as 5. The value distribution of pulse signal frequency $f = 50MHz$

,and control phase interference are uniformly and randomly dispersed within the range of 0 (non discrete), $\pm\pi/2$, $\pm\pi$ respectively. Fig. 2 shows the impact of different phase differences on the time domain cumulative average of the signal.

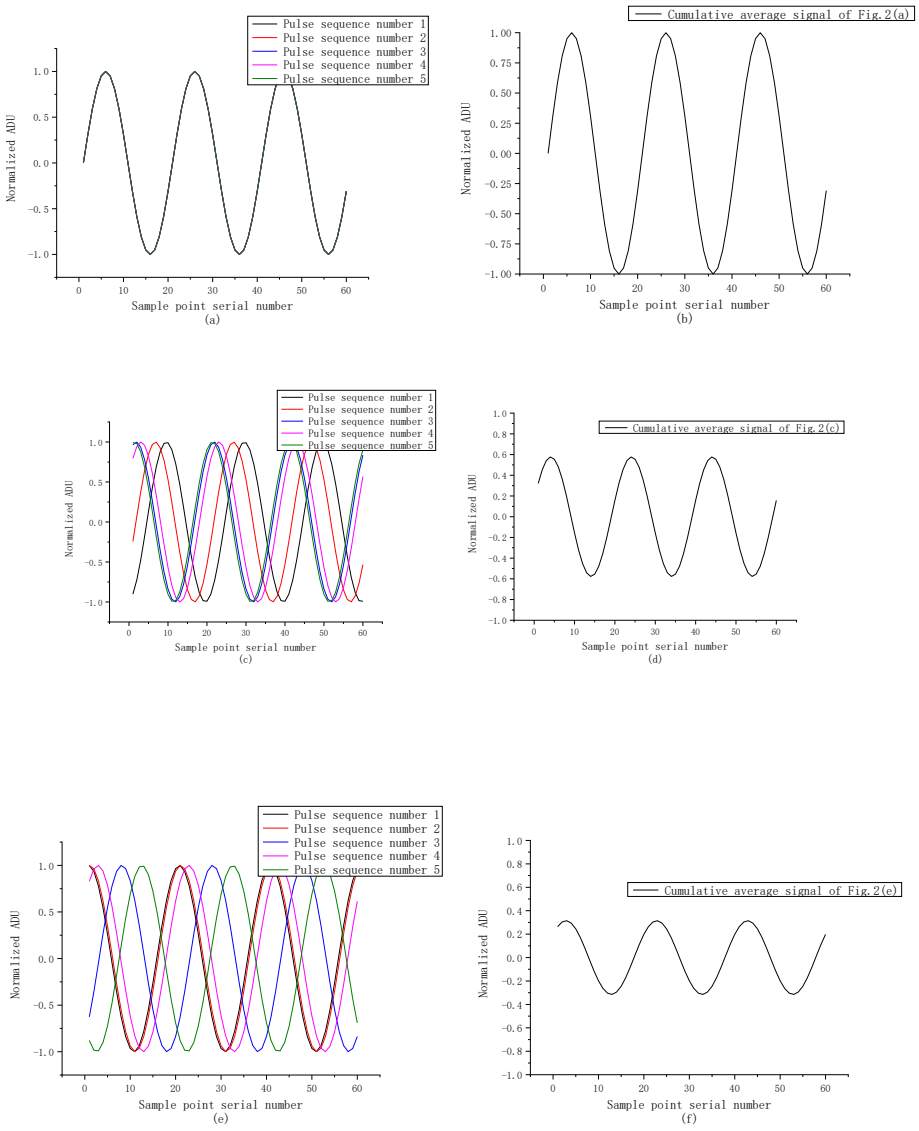

Fig. 2. Comparison of Effects of Different Phase Differences on Time Domain Cumulative Average of Pulse Signals, listed as: (a) Pulse group signals with non discrete phases; (b) Cumulative average of pulse group signals with non discrete phases; (c) Pulse group signals with uniformly discrete phases; (d) Cumulative average of pulse group signals with uniformly discrete phases; (e) Pulse group signals with uniformly discrete phases; (f) Cumulative average of pulse group signals with uniformly discrete phases.

It can be found that under the influence of phase interference, multi-pulse accumulated signals with constant frequency values but different phases are still sinusoidal waveforms with the same frequency, but the amplitude of direct accumulation in the time domain will be significantly weakened, and the more discrete the phases, the lower the superimposed amplitude.

3.3. Time domain signal shift alignment based on correlation coefficient

The correlation coefficient represents the correlation between two variables. The selected correlation coefficient is the Pearson correlation coefficient, which is calculated by dividing the covariance of two variables by the product of their respective standard deviations. The positive and negative sign correspondence of the correlation coefficient indicates that the greater the absolute value of the positive and negative correlation coefficients, the stronger their correlation. From a numerical perspective, the larger the coefficient correlation, the stronger the correlation between the positive correlations of the two variables.

Considering that the computational processing of phase detection for the initial phase of each pulse signal is too complex [17], a time domain signal shift alignment method based on correlation coefficients is proposed. This method first requires setting a reference equal to the length of the pulse signal, and then, based on the principle of maximizing the correlation coefficient, performing a forward and backward search calculation for shift alignment, and sequentially completing the shift operations for all pulses. Based on this, it is also possible to eliminate the initial phase difference, thereby improving the amplitude strength of the multi-pulse accumulation average signal.

At this point, consider the impact of amplitude noise. Although superposition averaging can eliminate amplitude noise to a certain extent, discrete phase distributions can also reduce the amplitude of useful signals, leading to a reduction in signal-to-noise ratio. Coherent accumulation refers to the superposition of signal amplitude taking into account the phase relationship between each received pulse. The signal strength will increase as the number of accumulation increases, while relatively independent signals will not linearly increase with accumulation. Compared to the non coherent accumulation of spectrum signals after superposition detection, it can effectively suppress noise, highlight the signal, and achieve a gain in signal-to-noise ratio. Through the line-by-line shift effect of the time domain alignment algorithm, the phase difference between different pulses of the final output signal of the detector is gradually reduced in multiple iterations, further enhancing the amplitude of the superimposed signal, and achieving signal-to-noise ratio gain.

3.4. Algorithm flow

Coherent accumulation algorithm based on time domain alignment is proposed to process the data segments corresponding to the distance gate to be measured. The specific operation steps of the algorithm are as follows:

Step 1: Divide the obtained pulse echo signal data by pulse sequence number to obtain an array K_{origin} of n row and N columns, where n is the total number of pulse groups and N is the single pulse distance gate length;

Step 2: Arithmetically average the signal arrays of n row and N column by row to obtain the signals of 1 row and N column, and use this as a reference signal for alignment;

Step 3: Take half of the number of intermediate frequency period points of the signal as the maximum allowable translation radius r, translate the selected distance gate data left and right, obtain the position with the largest correlation coefficient among the $2*r+1$ results, record the number of translation points, perform translation replacement operations on the corresponding lines of the signal array, and process them line by line;

Step 4: Perform the iterative operation according to the set number of times, and repeat the calculations in Step 2 and Step 3 to obtain the final aligned signal array K_{last} of n row and N columns;

Step 5: Arithmetically average the aligned signal array by row to obtain the aligned time domain signal, and in this time domain signal, select the corresponding range gate data according to the required detection distance for FFT to obtain the spectral data of the echo signal.

4. Numerical simulation verification under constant wind speed

When detecting a target with a constant velocity, the frequency of the echo signal will appear as a constant value because there is no change in velocity. When the constant speed is zero, the echo signal and the LO optical signal will have the same frequency. Note that the final output signal of the detector is

$$S_n = sin(2\pi ft + b_n) + a_n \tag{12}$$

In Equation (12), f is the output signal frequency, the numerical value is the same as the local oscillator frequency, t is a time series, n is the pulse sequence number, and a_n is the amplitude noise sequence of the corresponding pulse of equal length to t. Here, the amplitude noise is the Gaussian white noise with a specified root mean square, and b_n is the phase interference of the corresponding pulse. The phase changes of each group of pulses are different, and they are set to be uniformly dispersed within the range of $[-\pi, \pi]$.Set the sampling frequency to $1000MHz$, take the local oscillator frequency value as $80MHz$, that is, the output signal

frequency is $f = 80MHz$, and the pulse repetition frequency is $20kHz$. Set the range gate data starting point of the analog echo signal S_n to 300, and set the sampling points to 512. Select 10000 sets of pulse echo data and separately add different RMS amplitude noise effects to the array. Use the power spectrum information corresponding to each range gate in literature [18] and the phase detection system in literature [19] to align the initial phases of different pulses, and then directly average the corresponding signals of each range gate in the time domain. During spectrum transformation, the method of adding zeros is used to optimize spectrum resolution, The number of data sampling points after zeroing is 2048. The experimental results of the two algorithms for calculating the spectral value of the echo signal are shown in Fig. 3 (a-d). The algorithm in this paper uses a coherent accumulation algorithm based on time domain alignment to process and obtain the spectral value of the echo signal. The number of test samples is set to 100, that is, each test sample is sequentially used with 100 sets of pulse echo data, and the number of iterations of the algorithm is set to 10. The test results obtained are shown in Fig. 3 (e) and Fig. 3 (f). FFT is also used to compensate for zero to 2048 points, which is compared with the processing results of the above algorithm.

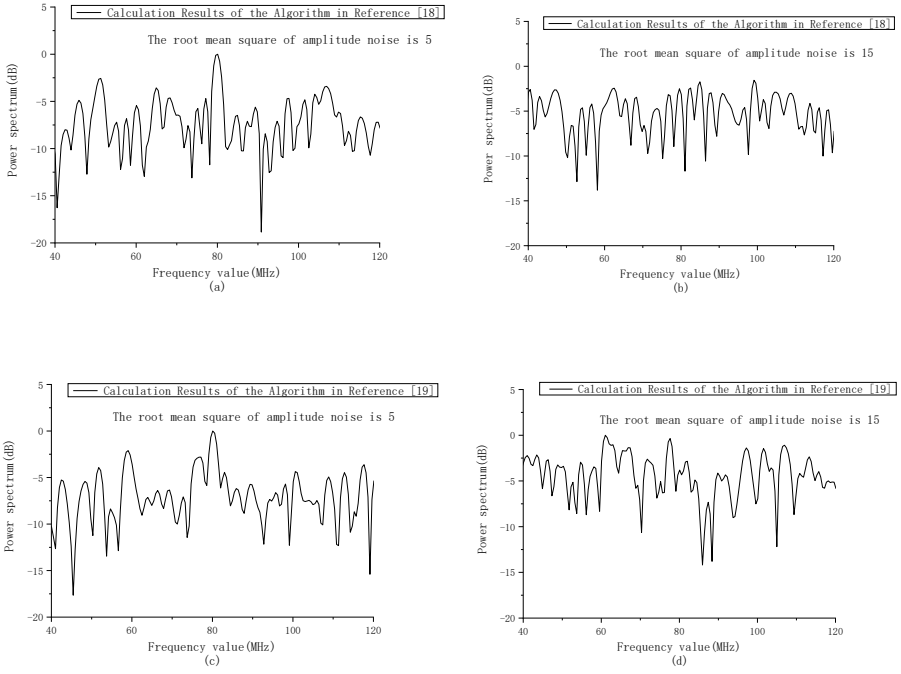

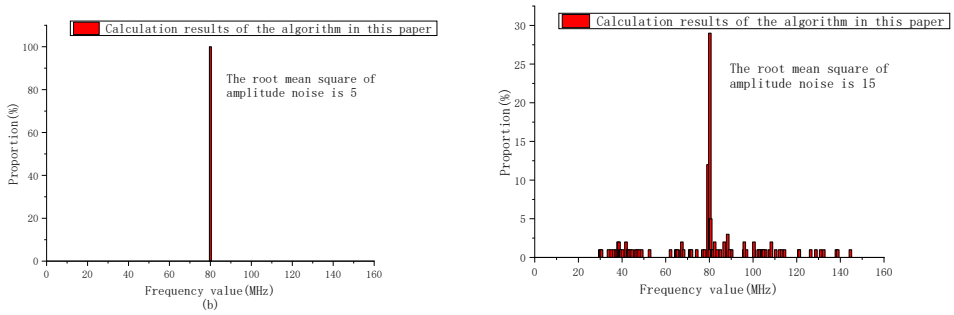

Fig. 3. Results of frequency values calculated by different algorithms when $f = 80MHz$ in numerical simulation. (a) Results of literature [18] algorithm when the root mean square of noise is 5; (b) Results of literature [18] algorithm when the root mean square of noise is 15; (c) Results of literature [19] algorithm when the root mean square of noise is 5; (d) Results of literature [19] algorithm when the root mean square of noise is 15; (e) Results of this algorithm when the root mean square of noise is 5; (f) Calculation results of the algorithm when the root mean square of noise is 15.

According to the test results in Fig. 3, when the noise interference gradually increases, the cumulative power spectrum information corresponding to each range gate used in literature [18] cannot achieve accurate detection. Literature [19] uses a phase detection system to align the initial phases of different pulses and directly average the corresponding signals of each range gate in the time domain to obtain relevant spectral information. This can improve the signal-to-noise ratio to a certain extent, but deviations can also occur when the noise interference is large. In practice, as the degree of noise interference increases, the probability of multiple frequencies appearing in the detection results will also increase. Combining the maximum likelihood criterion, that is, when randomly selecting n sets of sample observations from the model population, the most reasonable parameter estimator should maximize the probability of extracting the n sets of sample observations from the model. In this regard, the algorithm in this paper optimizes the signal to noise ratio by aligning the time domain signals based on correlation coefficients and accumulating them through alignment. Finally, the wind speed can be calculated at low signal to noise ratios.

For the processing results of the algorithm in this article, when the frequency of the echo signal obtained from one detection is set to be within the range of $f \pm 0.5MHz$, it is considered as effective detection. The detection ability of the corresponding wind measurement system algorithm is characterized by the proportion of the effective detection times to the total detection test times. The proportion of the effective detection times corresponding to Fig. 3 (e) is 100%, while the proportion of the effective detection times corresponding to Fig. 3 (f) is

41%. It can be seen that when amplitude noise interference gradually increases, multi-pulse accumulation signals with different phases will be submerged, and the algorithm in this paper has relatively superior detection capabilities under different signal-to-noise ratios. In the experiment, the effective detection times of the algorithm in this paper will decrease as the degree of noise interference increases, but combined with the maximum likelihood criterion, it will always remain in the form of maximum probability, and this result will be used as the detection of the final wind measurement system algorithm. Based on this, the algorithm in this paper eliminates initial phase differences through alignment operations in the signal time domain and improves the signal to noise ratio of the signal to achieve effective detection. It has a broad application prospect in processing coherent wind measurement data.

5. Measurement Test of Actual Atmospheric Radial Wind Speed

The radial wind speed of the actual atmospheric wind field is measured. The pulse laser center frequency of the built coherent wind measurement system is $80MHz$, the sampling frequency is set to $1000MHz$, the pulse repetition frequency is $20kHz$, and the starting distance of the data distance gate is set to 512 sampling points. In the experiment, the laser output direction is adjusted to the due south direction, and 150 consecutive sets of pulses are also selected as a sample test input. The total number of tests is set to 100. During spectrum transformation, the method of zeroing is used to optimize spectrum resolution. The number of data sampling points after zeroing is 2048. The iteration number of the algorithm in this article is set to 10, and the processing results of the statistical algorithm are shown in Fig. 4 (g-i). Fig. 4 (a-c) and Fig. 4 (d-f) show the test results using the literature [18] algorithm and literature [19] algorithm and zeroing to 2048 data sampling points, with a cumulative pulse count of 15000. Each column in Fig. 4 represents the solution of different algorithms to the same wind measurement data, and the interference of random noise in each column of test conditions from left to right will gradually worsen the signal to noise ratio.

Referring to Fig. 4, it can be seen that compared to other algorithms, the algorithm in this paper can clearly calculate wind speed information under different signal-to-noise ratios. In order to quantitatively characterize the accuracy of the processing results of this algorithm, Vaisala wind measurement data are used for comparison. Fix the Vaisala device 150 meters away from the laser emission point and let the laser path pass through the Vaisala wind measurement area to verify the performance of different algorithms in detecting actual atmospheric wind speed. During the test, adjust the output laser power to $300mW$.

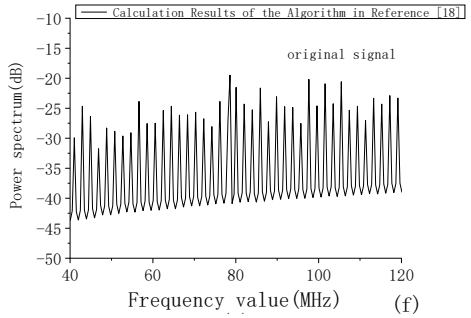
Calculation Results of the Algorithm in Reference [18]
original signal
Power spectrum(dB)
Frequency value(MHz)
(f)

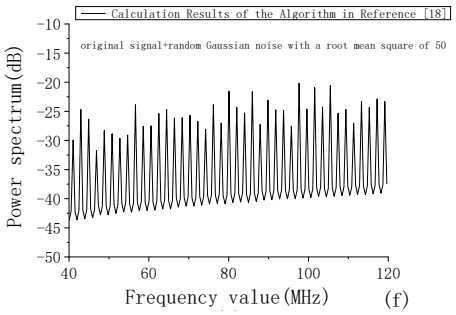
Calculation Results of the Algorithm in Reference [18]
original signal+random Gaussian noise with a root mean square of 50
Power spectrum(dB)
Frequency value(MHz)
(f)

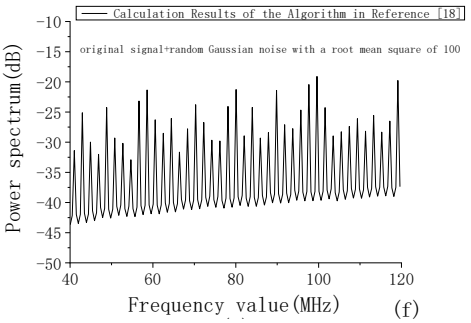
Calculation Results of the Algorithm in Reference [18]
original signal+random Gaussian noise with a root mean square of 100
Power spectrum(dB)
Frequency value(MHz)
(f)

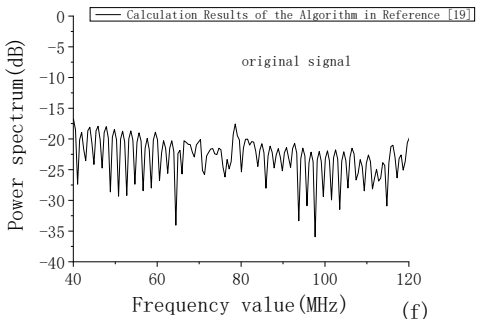
Calculation Results of the Algorithm in Reference [19]
original signal
Power spectrum(dB)
Frequency value(MHz)
(f)

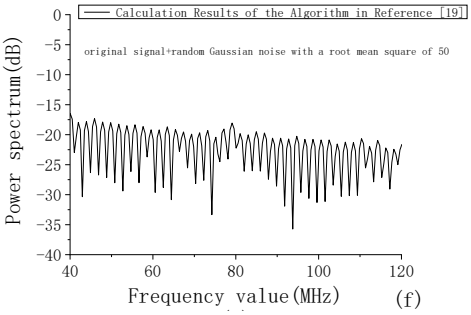
Calculation Results of the Algorithm in Reference [19]
original signal+random Gaussian noise with a root mean square of 50
Power spectrum(dB)
Frequency value(MHz)
(f)

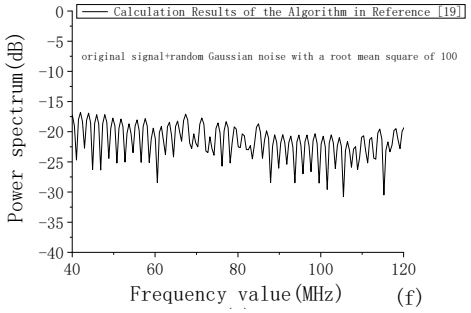
Calculation Results of the Algorithm in Reference [19]
original signal+random Gaussian noise with a root mean square of 100
Power spectrum(dB)
Frequency value(MHz)
(f)

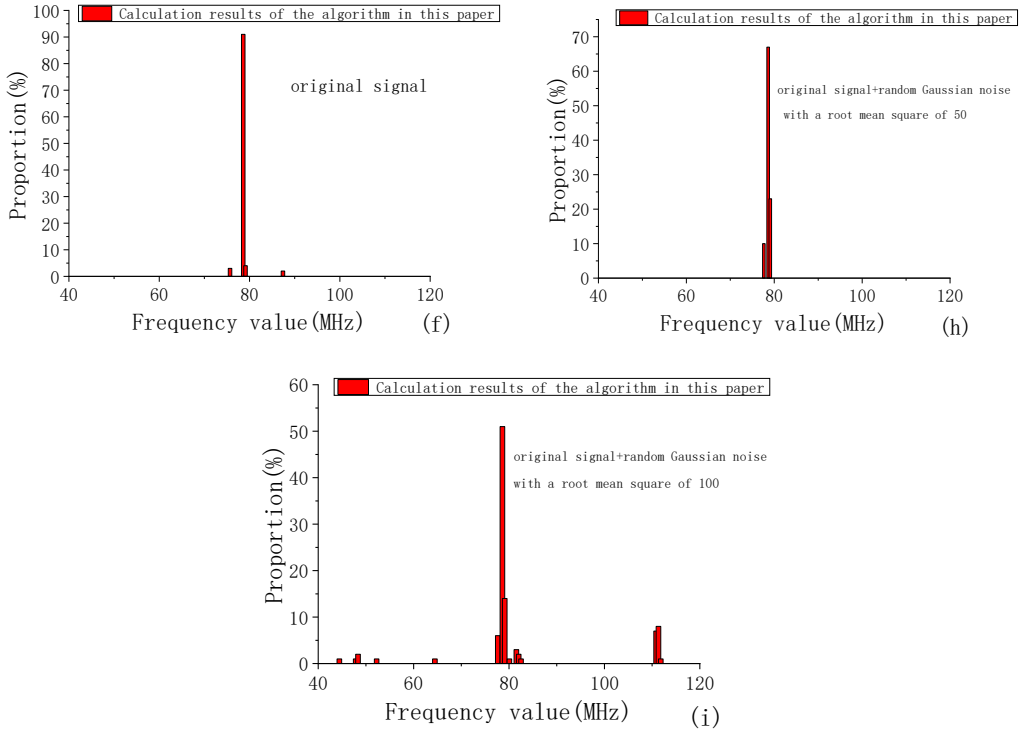

Fig. 4. Results of frequency values calculated by different algorithms in actual atmospheric exploration. (a-c) Results of calculations under different signal-to-noise ratios by literature [18] algorithms; (d-f) Results of calculations under different signal-to-noise ratios by literature [19] algorithms; (g-i) Results of calculations under different signal-to-noise ratios by this algorithm.

Correspondingly, read the wind speed data projected by Vaisala in the due north due south direction during the sampling period, and note that the due north direction is a positive value of the speed. You can calculate the wind speed at this time according to the algorithms in literature [18] and literature [19], and then use the maximum likelihood criterion to read the wind speed calculated by the algorithm in this article.

Using Vaisala's radial wind speed data as a standard, the wind speed data calculated by the above three algorithms are compared at different time periods, and the results are summarized in Table 1. It can be seen that the wind speed calculated by this algorithm is relatively consistent with Vaisala's radial wind speed data within the allowable range of test error.

Drawing on the results of multiple experiments presented in Table 1, the inability of the algorithm in reference [19] to effectively calculate wind speed can be attributed to the low laser emission power.

Table 1

Comparison between wind speed results calculated by different algorithms and Vaisala wind speed data

Period Number	Vaisala wind speed (m/s)	Results of algorithm in literature [18]		Results of algorithm in literature [19]		Results of algorithm in this paper	
		wind speed (m/s)	error (%)	wind speed (m/s)	error (%)	wind speed (m/s)	error (%)
1	-0.56	-0.32	43	\	\	-0.70	25
2	0.67	1.20	79	\	\	0.82	22
3	-0.90	0.82	191	\	\	-1.09	9
4	-0.91	-0.70	23	\	\	-0.70	23

This low power results in a poor signal - to - noise ratio. Consequently, when the signal - to - noise ratio of the echo signal drops below a certain threshold, the algorithm fails to effectively perform initial phase alignment.

The algorithm in reference [18], by virtue of employing over ten - thousand accumulations, can still resolve wind speed. Nevertheless, in most scenarios, significant deviations may occur. To measure the error between the predicted and actual values, the root mean square error (RMSE) and mean absolute error (MAE) are incorporated into the loss function. These are then utilized to calculate the difference between the actually measured wind speed and the wind speed detected by Vaisala [21]. By integrating multiple sets of measurement data, it is calculated that the root mean square relative error (RMSRE) between the algorithm in reference [18] and the corresponding Vaisala wind speed data ranges from 2.1 - 3.1 m/s. In contrast, the RMSRE variation range between the algorithm proposed in this paper and the corresponding Vaisala wind speed data is 1.3 - 1.9 m/s.

Currently, the RMSE value of the forecasting system (encompassing weather forecast and post - processing) lies between 1.5 and 2.5 m/s.When taking Vaisala wind speed as a reference, the error calculated by the algorithm in this paper has distinct advantages over traditional coherent accumulation algorithms. However, since zero - padding in the fast Fourier transform (FFT) does not augment useful information, it is infeasible to continuously enhance speed resolution and reduce errors merely by increasing the data zero - padding length. In subsequent experiments, the data processing algorithm will be further optimized. Comparatively, the algorithm in this article is more accurate in reflecting the real wind speed and can be effectively applied to the data processing of the atmospheric wind field measured by coherent laser wind measurement radar.

6. Conclusion

In response to the actual situation of relatively weak signal strength in coherent wind measurement pulsed laser radar data processing, a coherent

accumulation algorithm based on time domain alignment is proposed to retrieve wind speed information. The algorithm eliminates the difference in initial phase between different pulses through iterative alignment and eliminates the impact of random noise through multi-pulse accumulation. Finally, effective detection of echo signals and signal-to-noise ratio gain are achieved in experiments. In the future, the algorithm will be improved and supplemented by comparative tests of actual atmospheric wind speeds at different distances and Vaisala.

REFERENCES

[1] Rao Ruizhong. Light Propagation in Turbulent Atmosphere. Anhui: Science and Technology Press, 2005.

[2] Yu Yongjing, Li Liangxian, Xiong Magnum, et al. Study on the layout scheme of wind tower based on BP neural network. Journal of Solar Energy, 2021, 42(06):364-368.

[3] Liu Yang. Design of thermal anemometer based on temperature sensor array. Nanjing University of Information Engineering. 2021.

[4] Hou Tianhao. Design of an orthogonal wind pressure anemometer based on a multi rotor UAV platform. Nanjing University of Information Engineering. 2021.

[5] Zhang Pinghui. Non Doppler lidar wind measurement system based on convolutional neural networks. Optoelectron Laser, 2021, 32 (10):1039-1045.

[6] Gu Hao. Research on ultra-short term wind speed prediction algorithm based on wind acoustic radar technology. Zhengzhou University. 2021.

[7] Chen Zhen. Research on all fiber coherent wind lidar. Ocean University of China, 2015.

[8] Huffaker R M, Jelalian A V, Thompson J AL. Laser-Doppler system for detection of aircraft trailing vortices. Proceedings of the IEEE, 1970, 58: 322-326.

[9] Zhuang Peng, Shen Fahua, Wang Bangxin, et al. Research on Rayleigh Mie scattering wind lidar based on Fabry Perot interferometer. China Laser, 2020, 47 (12): 1210001.

[10] Zhou Yanzong, Wang Chong, Liu Yanping, et al. Research progress and application of coherent wind lidar. Laser and Optoelectronics Exhibition, 2019, 56(02):020001.

[11] Christer J. Karlsson, Fredrik Å. A. Olsson, Dietmar Letalick, and Michael Harris. All-fiber multifunction continuous-wave coherent laser radar at 1.55 mm for range, speed, vibration, and wind measurements. Applied Optics, 2000, 39(21):3716-3726.

[12] Zhou Yongsheng, Ma Xunpeng, Zhao Yiming, et al. Frequency estimation of weak signals from coherent wind lidar. Infrared and laser range, 2018, 47(03):0306001.

[13] Li Yunfei. 1.55 μ Research on data processing of m-coherent laser wind radar. Harbin Institute of Technology. 2018.

[14] Luo Tao. Research on Doppler shift estimation technology for coherent wind lidar. University of Electronic Science and Technology. 2022.

[15] Yang Wuhao, Zhang Pu, Yang Xinfeng, et al. Performance optimization analysis and experimental research of continuous mode coherent wind lidar. Acta Photonica Sinica, 2021, 50 (04): 89-98.

[16] Wang Pingchun. Research on Signal Processing and Algorithms of Coherent Wind Lidar. University of Science and Technology of China, 2018.

[17] Jin Xiaomei, Zhu Wenyue, Liu Qing, et al. Numerical modeling and simulation analysis of coherent wind lidar. Journal of Optics, 2021, 41(06):29-38.
[18] Diao Weifeng, Zhang Xin, Liu Jiqiao, et al. All fiber pulsed coherent lidar development for wind profiles measures in boundary layers. Chinese Optics Letters, 2014, 12 (07): 75-78.
[19] Fan Dongqian. Experimental study on pulse coherent accumulation technology of laser wind radar. Harbin Institute of Technology, 2015.
[20] Chen Zhen, Xin Fengxin, Wang Junyang, et al. Research on all fiber coherent Doppler continuous laser anemometer. Journal of Quantum Electronics, 2016, 33(02):243-248.
[21] C. Dica, C. -I. Dica, D. Vasiliu, G. Comanescu and M. Ungureanu, "Wind power short-term forecasting system," 2009 IEEE Bucharest PowerTech, Bucharest, Romania, 2009, pp. 1-7, doi: 10.1109/PTC.2009.5281941.